Bull. Chem. Soc. Ethiop. **2023**, 37(2), 265-276.
DOI: https://dx.doi.org/10.4314/bcse.v37i2.2

ISSN 1011-3924
Printed in Ethiopia
Online ISSN 1726-801X

GREEN SYNTHESIS OF SILICON DIOXIDE NANOPARTICLES AND L ARGININE@SILICON DIOXIDE NANOCOMPOSITES USING CELLULOSE OF *ZIZYPHUS SPINA-CHRISTI* ALONG WITH BIOLOGICAL EVALUATION

Ayyub Mojaddami[1,2], Hossein Chamkouri[3], Narges Chamkouri[4*], Zahra Koolivand[4] and Mohammad Panahimehr[5]

[1]Toxicology Research Center, Medical Basic Sciences Research Institute, Ahvaz Jundishapur University of Medical Sciences, Ahvaz, Iran
[2]Department of Medicinal Chemistry, School of Pharmacy, Ahvaz Jundishapur University of Medical Sciences, Ahvaz, Iran
[3]Department of Chemical Engineering and Petroleum, University of Tabriz, Iran
[4]Abadan University of Medical Sciences, Abadan, Iran
[5]Department of Chemistry, Faculty of Basic Science, Ayatollah Boroujerdi University, Boroujerd, Iran

(Received July 22, 2022; Revised November 28, 2022; Accepted November 30, 2022)

ABSTRACT. The recent research focused on the green synthesis of silicon dioxide nanoparticles, SiO_2@Cellulose of *Zizyphus Spina-Christi* nanocomposites, and L-Arginine@SiO_2@Cellulose of *Zizyphus Spina-Christi* nanocomposites using cellulose of *Zizyphus Spina-Christi* as a new green polymeric surfactant. The structures of nanoparticles and nanocomposites were characterized by different spectroscopy and microscopy techniques. Nanoparticles and nanocomposites were utilized to determine the concentration of chromium, cadmium, and lead in COVID-19 patients using double-vortex-ultrasonic assisted surfactant enhanced dispersive liquid-liquid microextraction. Mean recoveries of chromium, cadmium, and lead were obtained in the range of 86-98% with relative standard deviations below 4%. The advantages of the proposed method are green and novel polymer surfactant with low detection limit. Finally, antibacterial activities were investigated. The maximum inhibition zone of L-Arginine@SiO_2@Cellulose of *Zizyphus Spina-Christi* nanocomposites was obtained for *Staphylococcus Aureus* (21.9±0.4 mm). L-Arginine@SiO_2@Cellulose of *Zizyphus Spina-Christi* nanocomposites have low cytotoxicity against MCF-7 cancer cells. These results indicated the potential ability of L-Arginine@SiO_2@Cellulose of *Zizyphus Spina-Christi* nanocomposites in the determination of metal concentrations in biological samples along with good antibacterial properties and cytotoxic properties.

KEY WORDS: Green synthesis, Cellulose of *Zizyphus Spina-Christi*, Silicon dioxide nanoparticles, COVID-19, Biological activity

INTRODUCTION

Arginine is a semi-essential amino acid in the diet, as well as a naturally occurring amino acid in the body [1]. It is especially abundant in meats and nuts. In order to produce nitric oxide, L-arginine serves as a substrate for the enzyme nitric oxide synthase (NOS). Blood pressure is lowered by the production of nitric oxide in vascular endothelium. Additionally, the immune system uses arginine to produce nitric oxide for cell signaling or oxidative bactericide functions [2].

It has been suggested that poly L-arginine could be used for drug delivery, creates anticancer vaccines, regulates gene expression, and provide neuroprotection [3]. Researchers show that magnetic nanoparticles, such as Fe_3O_4 and SiO_2 coated with green components and biomolecules have antibacterial and cytotoxic properties as well as improve drug delivery systems. These nanocomposites have important roles in engineering processes and industry, coating phases, chemical polishing, biological activity, and evaluation of metals [4-6]. Both agriculture and

*Corresponding author. E-mail: narges.chamkouri@gmail.com

industry have significantly attributed to the raised heavy metals concentrations via sedicitsep, waste disposal, atmospheric deposition, smelter stacks, sewage sludge application, and fertilizer [7]. Moreover, metal absorption via vegetables and crops grown for consumption by humans is regularly detected [8, 9]. The elements copper (Cu), iron (Fe), cobalt (Co), and zinc (Zn) are found in trace amounts in living organisms and are vital for growth, development, health, and vitality. Whereas others, such as lead (Pb) and cadmium (Cd) are extremely noxious to humans, animals, and plants [10, 11]. The most important problem with heavy metals is that they are not metabolized in the body. After entering the body, metals are no longer excreted from the body and cause many side effects in the body [12, 13].

Escherichia coli (EC), *Proteus mirabilis (PM)*, and *Staphylococcus aureus (SA)* are pathogens which can cause a wide range of hospital- and community-acquired infections [14]. These organisms might lead to severe infections, especially in immunocompromised patients, that include urinary tract infections, pneumonia, diarrhea, and bloodstream infections. Besides, these organisms can easily acquire antibiotic resistance, making the search for compounds that can show antimicrobial activity against them very important [15].

Zizyphus Spina-Christi (ZSC), known as Sider in the Middle East, has potential applications in chemical, environmental, clinical, and biological studies. *Ziziphus* belongs to the genus Rhamnaceae (Buckthorn) and grows in Asia, Africa, and Southeast Europe. Copper nanoparticles can be fabricated with *Zizyphus Spina-Christi* fruit containing gallic acid, ellagic acid, tannins, leucoanthocyanins, and flavanol glycosides. [16].

Cellulose of *Zizyphus Spina-Christi* (CZSC) is used as the new green polymeric surfactant. This study aims to evaluate the simple and rapid method for preparation of silicon dioxide (SiO_2) nanoparticles, Arg@SiO_2@CZSCNCs, and SiO_2@CZSCNCs nanocomposites. These nanoparticles and nanocomposites were applied with a dual ultrasonic vortex to determine the levels of heavy metals in COVID-19 patients. In the first step, the one-factor-at-a time (OFAT) method was used for the screening parameters. Significant variables were selected and optimized in the second step using Box–Behnken Design (BBD). Besides, BBD-DVUESDLLME was applied to optimize and determine the concentrations of Cr, Cd, and Pb in COVID-19 patients by graphite furnace atomic absorption spectroscopy (GFAAS). Moreover, green nanocomposites were evaluated against antibacterial activity and cytotoxic properties. The antibacterial activities of CZSC, SiO_2@CZSCNCs, and Arg@SiO_2@CZSCNCs against *Escherichia coli (EC)*, *Proteus mirabilis (PM)*, and *Staphylococcus aureus (SA)* were evaluated. The MTT assay was used to study the cytotoxic properties of the MCF-7 breast cell line and the normal cell. SiO_2@CZSCNCs loaded with L-arginine as a drug delivery system was evaluated by high-performance liquid chromatography (HPLC).

EXPERIMENTAL

Chemicals and bacterial strains

All reagents were purchased from Sigma–Aldrich (Darmstadt, Germany). For determination of heavy metal levels, blood samples were collected and transferred to test tubes and then serum was isolated and determined. In the current work, 115 COVID-19 patients participated along with 31 healthy people as a control group. All participants were checked for COVID-19 using RT-PCR followed by hospitalization at the *Taleghani* Hospital of Abadan Medical Sciences University in south west of Iran during September to November 2020. Finally, concentration levels of Cr, Pb and Cd were determined in COVID-19 patients and compared to the control group by graphite furnace atomic absorption spectrometry (Agilent, 240 Z). In this work, *Escherichia coli* strain ATCC25922, *Staphylococcus aureus* strain ATCC25923, and *Proteus mirabilis* strain ATCC7002 were used.

Phytochemical analysis of CZSC

CZSC was collected from Abadan, Khuzestan province, south west of Iran. The leaves were shade dried and powdered by a grinding mixer. The ZSC was washed with distilled water and dried at ambient temperature. CZSC extract evaluation for its phytochemical content indicated that it has alkaloids, phenols, flavonoids, glycosides, tannins, terpenoids, and saponins.

Biosynthesis and characterization of nanoparticles and nanocomposites

CZSC@CZSCNCs were prepared by adding 0.05 g of CZSC to ethanol under ultrasound and adjusting pH = 9 with NH_3 25% v/v. Finally, ethyl silicate was added dropwise to the solution at room temperature. For preparation of Arg@SiO_2@CZSCNC$_S$, 0.02 g SiO_2@CZSCNCs was added into 50 µL of L-Arginine (10 mmol) that was dissolved in methanol under ultrasound.

Different spectroscopic and microscopic techniques were used to characterize nanoparticles and nanocomposite, including, UV-Visible spectroscopy (UV-Vis), field emission scanning electron microscopy (FESEM), transmission electron microscopy (TEM), X-ray diffraction (XRD), and Fourier-transform infrared spectroscopy (FT-IR). The absorption spectra were investigated by the UV–Vis double beam spectrophotometer Cecil 7500. FESEM and TEM were used to investigate morphological and structural properties of nanoparticles and nanocomposite. The functional group were evaluated by FTIR (Perkin Elmer) in the 400-4000 cm^{-1} wavelength range.

Evaluation of Cr, Cd and Pb levels

200 µL of the blood sample was mixed with 200 µL of nitric acid (HNO_3, 65% w/w), 200 µL of hydrochloric acid (HCl, 37% w/w), and 100 µL of the hydrogen peroxide (H_2O_2), and then was poured into the digestion vessel. Finally, the levels of Cr, Cd, and Pb after the microwave digestion were determined by graphite furnace atomic absorption spectroscopy (GFAAS). 1% HNO_3 was used to dilute the dried samples. The samples were then mixed with 200 µL of ammonia solution. As dispersed solvents, mixed samples were added to 1-butanol (300 µL, 1% v/v) and Arg@SiO_2@CZSCNCs as a novel green surfactant (200 µL). The samples were mixed twice using a vortex and ultrasonic water bath at 30 °C for 4 min. Finally, the concentrations of Cd, Cr, and Pb were determined.

Evaluation of antibacterial activities

The antibacterial activity of CZSCNCs, SiO_2@CZSCNCs, and Arg@SiO_2@CZSCNCs against *Staphylococcus aureus* (SA), *Proteus mirabilis* (PM), and *Escherichia coli* (EC) were evaluated by the agar disk diffusion method. Bacterial suspensions were prepared and used at 0.5 McFarland to inoculate the plates for 24 h at 37 °C as reference method.

In vitro release of L-arginine from Arg@SiO_2@CZSCNC$_S$

Release of L-Arginine from Arg@SiO_2@CZSCNC$_S$ was evaluated by high-performance liquid chromatography (HPLC, Agilent) with methanol and acetonitrile as solvents.

One-factor-at-a time method (OFAT) and Box-Behnken design (BBD)

Different factors, such as the volume of sample, the volume of 1-butanol, and the volume of surfactant were evaluated using OFAT and optimized by BBD. In the first step, OFAT was used as screening parameters, and significant factors were obtained. Finally, the remaining parameters obtained by OFAT were optimized by BBD.

RESULTS AND DISCUSSION

Characterization of nanocomposite

The FT-IR spectra (Figure 1) was employed to recognize the interaction between the molecule of CZSC(a), SiO_2@CZSCNCs (b), and Arg@SiO_2@CZSCNCs (c). Strong peaks at 3451 cm^{-1} and 3548 cm^{-1}, in all spectra, are related to the hydroxyl group (O-H). Peaks emerging at 2925 and 2850 cm^{-1} are correlated to the symmetric and asymmetric stretching methylene vibration groups (CH_2). Sharp peaks at 1635 and 1724 cm^{-1} are related to stretching vibration of C=O bonds. The peak at 1075 cm^{-1} in all spectra is attributed to Si–O stretching vibrations. Similarly, stretching vibrations of C-N in the spectrum of FT-IR appeared at 1327 cm^{-1}. Furthermore, the peaks at 1257, 1123, 806 and 670 cm^{-1} are related to C-O as stretching groups, C-O as secondary alcohol, C=C, and C-H, respectively. The previous phytochemical analyses and reduction of CZS were validated by these functional groups. Moreover, the reduction and stability of nanometals, as well as the inhibition of aggregation, were validated by these functional groups.

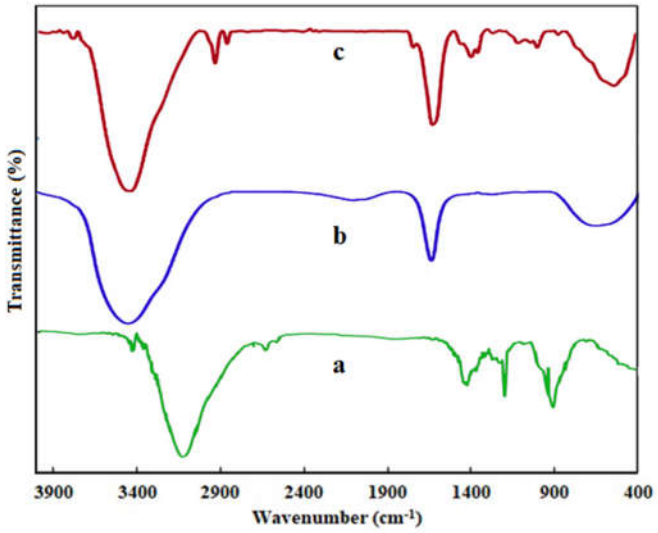

Figure 1. FT-IR spectra of CZSC (a), SiO_2 @ CZSCNCs (b), and Arg@SiO_2@CZSCNCs (c).

Figure 2(a-c) showed the XRD pattern of SiO_2, SiO_2@CZSCNCs, and Arg@SiO_2@CZSCNCs. The XRD peaks, as the index of crystallite purity, confirmed the formation of the nanocomposite. By analyzing XRD patterns of SiO_2, silica formation was identified and confirmed [4, 6]. XRD pattern were also in line with the UV–Vis spectrophotometric, TEM, and FESEM-EDS. The average crystallite sizes with Miller indices of SiO_2@CZSCNCs, and Arg@SiO_2@CZSCNCs observed at 220°, 311°, 400°, 422°, 511°, and 440°, respectively. The Miller indices demonstrated that the composite was successfully biosynthesized [6, 17].

Figure 2(d-e) represented UV-Visible spectra of green polymer CZSC, SiO_2@CZSCNCs, and Arg@SiO_2@CZSCNCs in the 300–900 nm wavelength range. In general, Arg@SiO_2@CZSCNCs display a peak of absorption in the 320–480 nm wavelength range that indicated presence of L-arginine in nanocomposite structure. The UV-Vis spectrum at 398 and 480 nm confirmed the

biosynthesis of SiO_2@CZSCNCs and Arg@SiO_2@CZSCNCs, respectively. This clarified the blue alteration in the optical peak of absorption as the L-arginine concentration. The alteration towards the higher wavelength side (red shift) similarly shows that size of SiO_2NPs is increasing as the concentration of CZSC is decreasing. Additionally, it is well-known from UV-Vis spectra that the absorption intensity is reduced through the raise of L-arginine concentration, which is contributed to a decrease in the concentration of SiO_2@CZSCNCs.

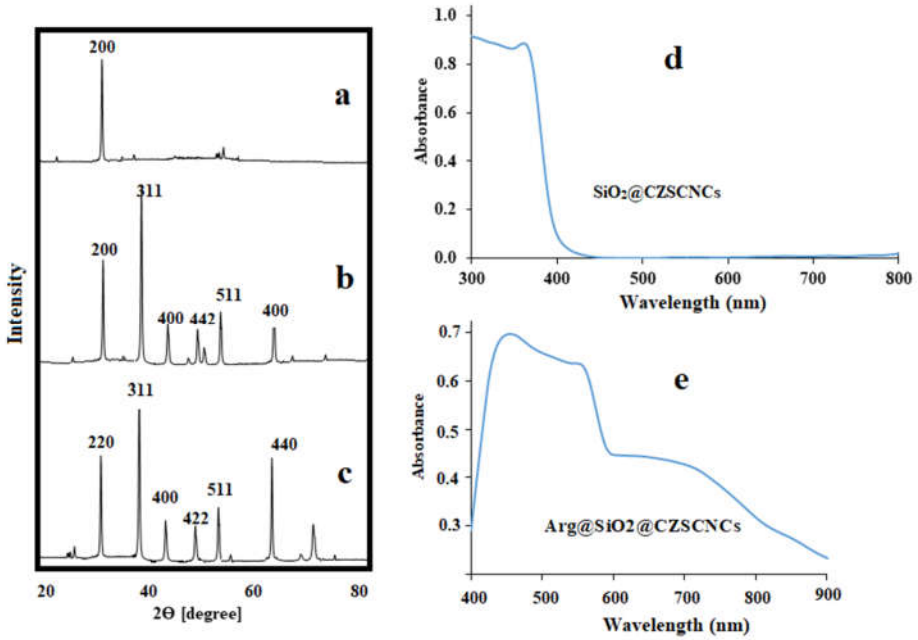

Figure 2. XRD of SiO_2 (a), SiO_2@CZSCNCs (b), and Arg@SiO_2@CZSCNCs (c) UV-Vis spectra of SiO_2@CZSCNCs (d), and Arg@SiO_2@CZSCNCs (e).

Morphology

25 nm average size and spherical-like shapes of nanoparticles was achieved from TEM and FESEM analysis. FESEM and TEM images displayed SiO_2@CZSCNCs stabilized in L-arginine. Figure 3c characterize SiO_2 stabilized in CZSCNCs and Figure 3d demonstrates corresponding distribution of particle size. FESEM images have been applied to investigate the morphology and structure of the Arg@SiO_2@CZSCNCs. Therefore, Images exposed that the SiO_2@CZSCNCs had the spherical particles with uniform morphology (Figure 3e-f). The morphological and structural study supported through TEM and FESEM analysis, verified that the size of SiO_2@CZSCNCs is not changed in the presence of L-arginine. The research reports showed that the concentration of stabilizer has a momentous effect on the size of particles. Sardar and coworkers [18] have perceived contradictory report. They have shown that the nanoparticles size increased from 2.6 to 4.3 nm as the concentration of stabilizer raised.

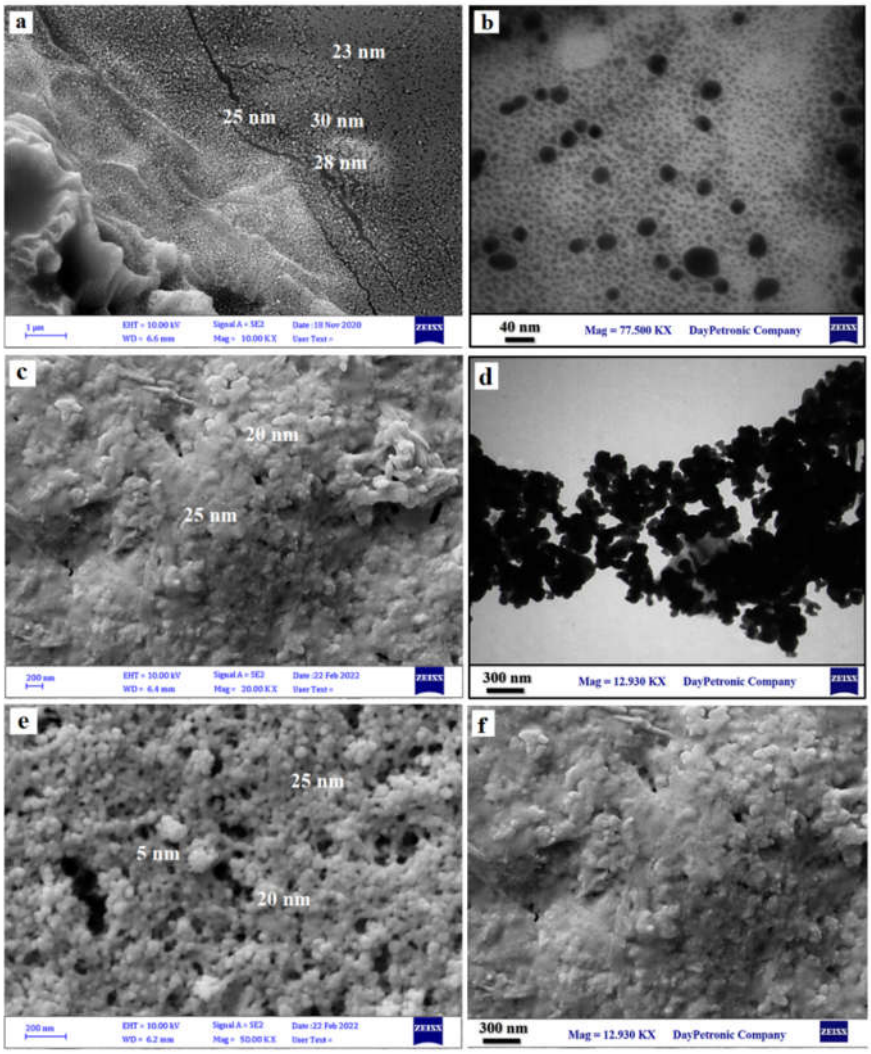

Figure 3. FESEM (a) and TEM (b) images of ZSCNCs, FESEM (c) and TEM (d) images of SiO_2@CZSCNCs, FESEM (e) and TEM (f) images of Arg@SiO_2@CZSCNCs.

The average size distribution of nanoparticles is revealed in Figure 4a. The content of elements of SiO_2@CZSCNCs and Arg@SiO_2@CZSCNCs confirmed through energy-dispersive X-ray spectroscopy (EDS) investigation (Figure 4b-c). The diagram of EDS of the nanocomposite is revealed in Figure 4(b-c). The result of EDS displayed the existence of C (Carbon), O (oxygen), and Si (silica) with a high percentage (52.4 % and 82 %) along with strong peaks for O and Si around 1, 2.1 keV, respectively. these results confirmed the formation of SiO_2@CZSCNCs and Arg@SiO_2@CZSCNCs.

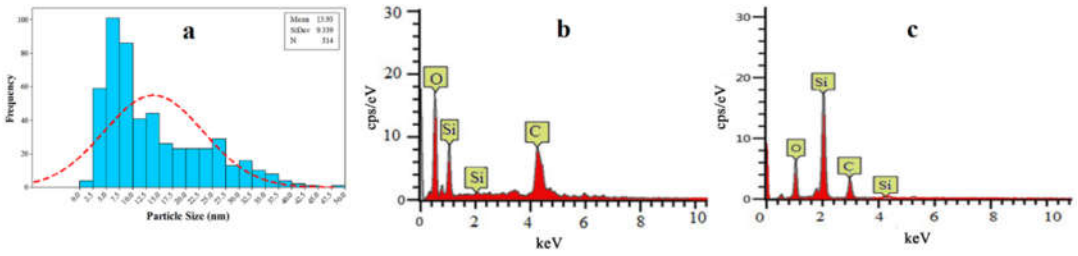

Figure 4. Average size distribution of Arg@SiO_2@CZSCNCs (a) and EDS of the SiO_2@CZSCNCs (b) and Arg@SiO_2@CZSCNCs (c).

Interactions between factors

In three-dimensional plots of the response surface, the interaction between two factors is presented at a given period while keeping another factor constant (Figure 5). This clarified the interaction between dissimilar variables. In fact, the contact between V sample and V surfactant (ZSC) shows the relation in which at both limits the reaction was low, and at 40 and 300, the reaction was precisely high showing a very acceptable contour (Figure 5a). The contact between V_{sample} and $V_{1\text{-butanol}}$ exposed a relation in which an acceptable contour was advanced. At the two normal ranges of factors, the reaction was worrying (Figure 5b). There was contact between $V_{1\text{-butanol}}$ and $V_{Surfactant\ (ZSC)}$. At all aspects, the destruction is very low, on the other hand, at the surfactant volume of 300, the destruction should be extra effective, therefore giving an actual acceptable curve (Figure 5c).

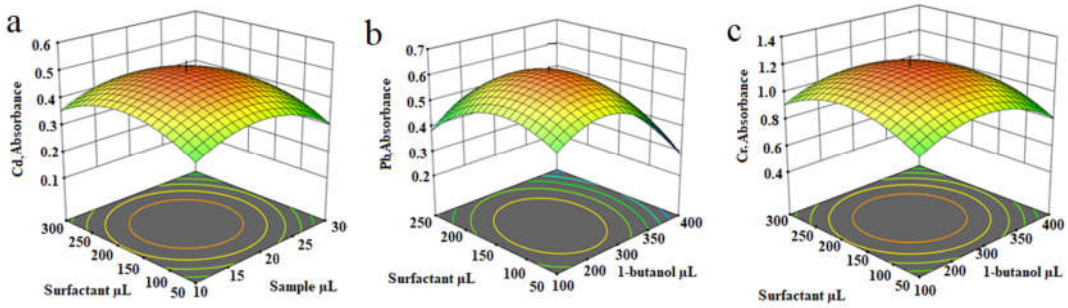

Figure 5. Optimization volume of sample (a), volume of 1-butanol as dispersive solvent (b), and volume of surfactant (c) by one-factor-at-a time method.

According to OFAT results, three independent factors including the volume of sample (X1), the volume of 1-butanol (X2), and the volume of surfactant (X3) were significant. In the BBD scheme, these variables were further evaluated. The factors are given in Table 1.

As a result, there is a linear relationship between the responses of heavy metals with the change of variables to obtain the optimal experimental conditions. The answers and variables tested are related by the equation. R^2 of the equation was equal to 0.89, and the volume of 1-butanol and surfactant were significant factors. The response level diagram is shown in Figure 6(a-c). Volume of sample (X1 = 25 µL), volume of 1-butanol (X2 = 300 (µL), and volume of surfactant (X3 = 200 µL) were determined.

Table 1. Factors and their levels in box benken design.

Factors	Level		
	Low	Center	High
	-1	0	1
V_{sample} (X1)	10	25	40
$V_{1\text{-butanol}}$ (X2)	100	300	500
$V_{Surfactant}$ (X3)	100	200	300

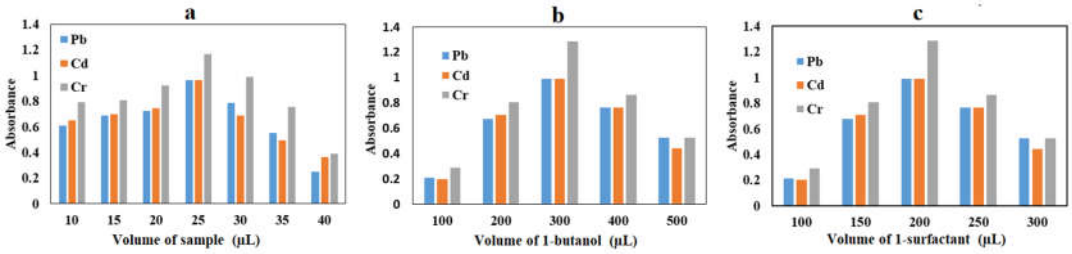

Figure 6. Optimization of the volume of sample (a), the volume of 1-butanol as a dispersive solvent (b), and the volume of surfactant (c) using the one-factor-at-a-time method.

Determination of the concentrations of Pb, Cr, and Cd

Concentrations of heavy elements (Cr, Pb, and Cd) in COVID-19 patients (n = 115) and healthy control (n = 31) were determined. All patients have ages between 19 to 50 years. The symptoms of the patients were classified as mild, moderate, and severe. 69.5% of the COVID-19 patients had mild symptoms, 17.4% of patients were with moderate symptoms, and 13.1% of them were divided as severe. As results in Table 2, the mean concentration of Cr, Cd, and Pb were 220.2±14.3, 0.11±0.03, and 9.2±2.5 $\mu g\, dL^{-1}$. The concentration of Pb and Cd were higher in COVID-19 patients in comparison with the control group, while Cr showed no significant difference. Several studies have indicated an association between heavy metals such as Pb and Cd exposure levels and impaired respiratory function and pulmonary function [19]. Pb and Cd exposure induced susceptibility to viral infections, inflammation and toxicity, lung remodeling, fibrosis, and apoptosis in A549 cells [14, 20].

Validation of BBD-DVUESDLLME - GFAAS

Validation of DVUDLLME-GFAAS was applied to determine the concentration of Pb, Cd, and Pb. To evaluate the method, the relative standard deviation (RSD), the limit of detection (LOD), the limit of quantification (LOQ), and the linear working range were calculated. Mean recoveries of Cr, Cd, and Pb were obtained in the range of 86-98%. The relative standard deviation (RSD) of DVUDLLME-GFAAS was below 4%. The advantages of the DVUESDLLME-GFAAS include wide range of dynamic performance, low consumption of solvents, high recoveries, and reproducible sample extraction with good LODs. Figure of merit DVUESDLLME-GFAAS are presented in Table 2.

Table 2. Mean concentration of Cr, Pb and Cd (μg dL^{-1}) in COVID-19 patient and control groups, and figure of merit for determination of heavy metals.

Element	COVID-19 group (Mean conc. ± SD)	Control group (Mean conc.±SD)	LOD (μg dL^{-1})	Dynamic range	LOQ	RSD%
Cd	0.11 ± 0.03	0.035 ± 0.004	0.05	0.01-5	0.2	2.1
Pb	9.2 ± 2.5	1.93 ± 0.01	1.3	0.05-25	3.3	3.5
Cr	220.2 ± 14.3	219.4 ± 8.6	141.2	100-250	218.1	2.8

Antibacterial activities

The antibacterial activity of CZSC, SiO_2@CZSCNCs, and Arg@SiO_2@CZSCNCs against *Staphylococcus aureus (SA)*, *Proteus mirabilis (PM)*, and *Escherichia coli (EC)* were evaluated at different concentrations (50-500 μgL^{-1}) using disk diffusion method (Figure 7a-d).

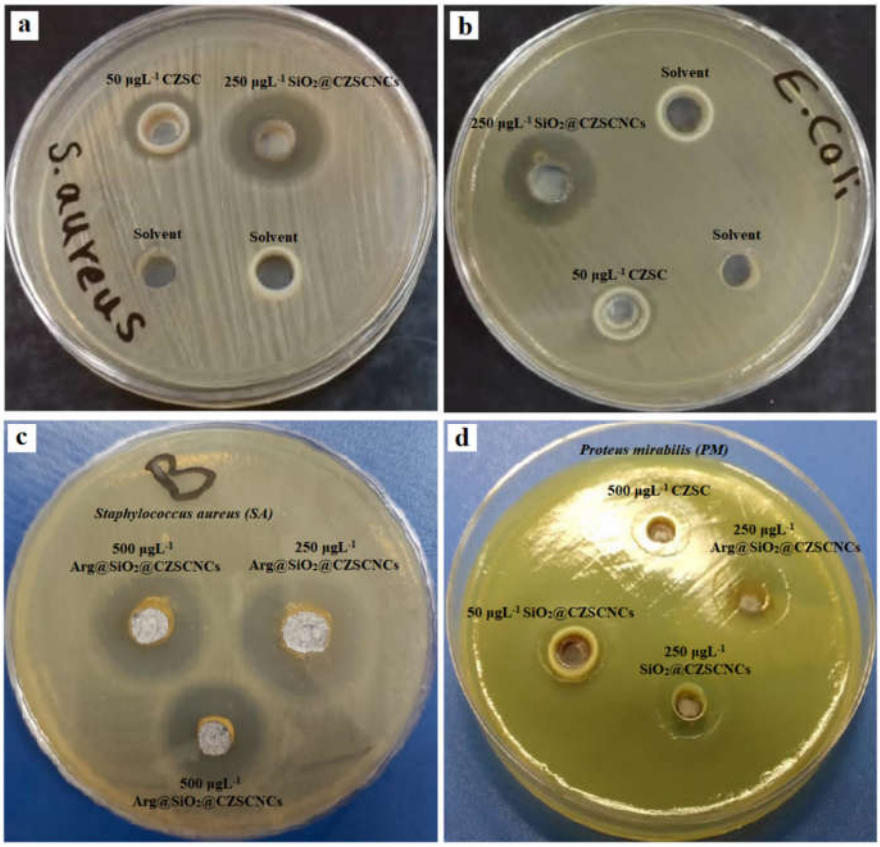

Figure 7. Zone of inhibition of CZSC, SiO_2@CZSCNCs, and Arg@SiO_2@CZSCNCs for EC, SA, and PM at different concentrations.

Zones of inhibition against EC, SA and PM at different concentrations were summarized in Table 3. This bacterial growth inhibition could be due to the damage to the cell membrane [18, 21]. This damage can cause pores in the bacterial membrane through interaction with this negatively charged structure, especially in the presence of moisture [22, 23]. The production of reactive oxygen species (ROS) by these nanoparticles is another reason for killing bacteria [24]. Generally, different mechanisms contribute to nanoparticle antibacterial activity, including inhibition of cell wall synthesis and membrane permeability, which lead to cellular component leakage, disruption of energy transfer, photocatalysis, enzyme inhibition, and disruption of DNA and protein production [25-27]. The high antibacterial activity of nanocomposite coated with L-arginine and alginate was obtained against *SA* and *EC* [6]. Amirnejat *et al.* investigated the antibacterial activities of iron oxide nanoparticles (SPIONs) coated with L-arginine (Arg) against both Gram-positive and Gram-negative bacteria. high antibacterial activity was obtained for *SA* and *EC* [28]. Magnetic silica nanocomposites (MSNCs) showed potential applications in drug delivery agents and antibacterial activity [29].

Table 3. Zone of inhibition against *Escherichia coli* (EC), *Staphylococcus aureus* (SA) and *Proteus mirabilis (*PM) at different concentrations.

Sample		Zone of inhibition (mm)		
	Conc. μgL^{-1}	EC	SA	PM
CZSC	50	4.1 ± 0.2	5.0 ± 0.3	5.1 ± 0.1
	100	6.2 ± 0.1	5.2 ± 0.3	5.2 ± 0.2
	250	8.3 ± 0.3	5.4 ± 0.1	6.5 ± 0.3
	500	9.5 ± 0.2	7.2 ± 0.5	7.3 ± 0.2
Arg@SiO_2@CZS CNCs	50	9.2 ± 0.4	10.4 ± 0.3	10.1 ± 0.2
	100	9.3 ± 0.3	13.2 ± 0.1	12.5 ± 0.6
	250	14.4 ± 0.6	21.9 ± 0.4	16.4 ± 0.3
	500	15.6 ± 0.1	21.1 ± 0.5	16.1 ± 0.1
SiO_2@CZSCNCs	50	9.1 ± 0.2	9.3 ± 0.4	9.2 ± 0.1
	100	11.3 ± 0.1	10.2 ± 0.6	9.3 ± 0.1
	250	13.5 ± 0.4	15.6 ± 0.4	14.5 ± 0.4
	500	12.9 ± 0.1	15.2 ± 0.8	13.1 ± 0.6

Evaluation of cytotoxicity

The cytotoxic activity of the CZSC, SiO_2@CZSCNCs, Arg@SiO_2@CZSCNCs, and free L-arginine were evaluated against MCF-7 cell line. Generally, Arg@SiO_2@CZSCNCs showed minimum cytotoxic effects on MCF-7 cell line compared to normal cell line. Bharathi *et al.* synthesized SiO_2–ZnO nanocomposite using *Dictyota bartayresiana* extract and evaluated its cytotoxic and antibacterial properties [22]. Zamani *et al.* investigated nano-$SnCl_4$.SiO_2 against MCF7 and A549 cell lines. The cytotoxic activities were moderate to weak with IC_{50} values of 656.4±10.8 μM and 635.7±1.9 μM for MCF-7 and A549, respectively [23].

CONCLUSION

In this work, a simple and rapid method used to investigate the biosynthesis of SiO_2@CZSCNCs, and Arg@SiO_2@CZSCNCs by cellulose of *Zizyphus Spina-Christi* (CZSC) as the new green polymeric surfactant. Arg@SiO_2@CZSCNCs utilized to evaluate the concentration of chromium (Cr), cadmium (Cd), and lead (Pb) by double-vortex-ultrasonic assisted surfactant enhanced dispersive liquid-liquid micro extraction (DVUESDLLME) in 115 patients with COVID-19 and 31 healthy people as a control group. According to the results, Pb and Cd were higher in the patient group in comparison with the control group, while Cr showed no significant difference

between them. Moreover, antibacterial activities of CZSC, SiO_2@CZSCNCs, and Arg@SiO_2@CZSCNCs were evaluated against *Escherichia coli (EC)*, *Proteus mirabilis (PM)*, and *Staphylococcus aureus (SA)*. The maximum inhibition zone for Arg@SiO_2@CZSCNCs against *SA* was 21.9±0.4 mm at a concentration of 250 μgmL^{-1}. Arg@SiO_2@CZSCNCs as a drug delivery system reduced the cytotoxicity of MCF-7 breast cancer cells. The Arg@SiO_2@CZSCNCs were successfully used to determine serum heavy metals with antibacterial and cytotoxic properties.

ACKNOWLEDGEMENT

This study was financially supported by Abadan University of Medical Sciences (Grant NO. 1400U-1281, ethics: IR.ABADANUMS.REC.1400.051).

REFERENCES

1. Noori, A.; Hoseinpour, M.; Kolivand, S.; Lotfibakhshaiesh, N.; Azami, M.; Ai, J.; Ebrahimi-Barough, S. Synergy effects of copper and L-arginine on osteogenic, angiogenic, and antibacterial activities. *Tissue Cell* **2022**, 77, 101849.
2. McRae, M.P. Therapeutic benefits of L-arginine: An umbrella review of meta-analyses. *J. Chiropr. Med.* **2016**, 15, 184-189.
3. Sepahi, M.; Jalal, R.; Mashreghi, M. Antibacterial activity of poly-L-arginine under different conditions. *Iran. J. Microbiol.* **2017**, 9, 103.
4. Gilanizadeh, M.; Zeynizadeh, B. Synthesis of acridinediones and biscoumarins using Fe_3O_4@ SiO_2@Ni–Zn–Fe LDH as an efficient magnetically recoverable mesoporous catalyst. *Polycyclic Aromat. Compd.* **2021**, 41, 15-32.
5. Hamadamin, S.I.; Anwer, S.S.; Abdulkareem, P.M.; Sdiq, K.H. Biogenic synthesis of ferrous (III) oxide and Fe_3O_4/SiO_2 using Chlorella sp. and its adsorption properties of water contaminated with copper(II) ions. *Bull. Chem. Soc. Ethiop.* **2022**, 36, 585-596.
6. Marsooli, M.A.; Nasrabadi, M.R.; Fasihi-Ramandi, M.; Adib, K.; Eghbali, M.; Pourmasoud, S.; Ahmadi, F.; Sohouli, E.; Nasab, A.S.; Mirhosseini, S.A. Preparation of $Fe_3O_4/SiO_2/TiO_2/PrVO_4$ nanocomposite in various molar ratios: Investigation on photocatalytic performance on organic contaminate and bacterial environments, and anti-cancer properties. *Polyhedron* **2020**, 176, 114239.
7. Chakraborty, R.; Asthana, A.; Singh, A.K.; Jain, B.; Susan, A.B.H. Adsorption of heavy metal ions by various low-cost adsorbents: a review. *Int. J. Environ. Anal. Chem.* **2022**, 102, 342-379.
8. Singh, A.; Pal, D.B.; Mohammad, A.; Alhazmi, A.; Haque, S.; Yoon, T.; Srivastava, N.; Gupta, V.K. Biological remediation technologies for dyes and heavy metals in wastewater treatment: New insight. *Bioresour. Technol.* **2022**, 343, 126154.
9. Hua, M.; Zhang, S.; Pan, B.; Zhang, W.; Lv, L.; Zhang, Q. Heavy metal removal from water/wastewater by nanosized metal oxides: a review. *J. Hazard. Mater.* **2012**, 211, 317-331.
10. Chai, W.S.; Cheun, J.Y.; Kumar, P.S.; Mubashir, M.; Majeed, Z.; Banat, F.; Ho, S.-H.; Show, P.L. A review on conventional and novel materials towards heavy metal adsorption in wastewater treatment application. *J. Cleaner Prod.* **2021**, 296, 126589.
11. Meligy, A.M.A. Comparative study of element contents in seven isolates of entomopathogenic nematodes. *Egypt. J. Biol. Pest Control.* **2018**, 28, 1-7.
12. Ying, X.; Fang, Z. Experimental research on heavy metal wastewater treatment with dipropyl dithiophosphate. *J. Hazard. Mater.* **2006**, 137, 1636-1642.
13. Qasem, N.A.A.; Mohammed, R.H.; Lawal, D.U. Removal of heavy metal ions from wastewater: A comprehensive and critical review. *Npj Clean Water* **2021**, 4, 1-15.

14. Shurin, M.R.; Naiditch, H.; Gutkin, D.W.; Umansky, V.; Shurin, G.V. ChemoImmunoModulation: Immune regulation by the antineoplastic chemotherapeutic agents. *Curr. Med. Chem.* **2012**, 19, 1792-1803.
15. Jomehzadeh, N.; Koolivand, Z.; Dahdouh, E.; Akbari, A.; Zahedi, A.; Chamkouri, N. Investigating in-vitro antimicrobial activity, biosynthesis, and characterization of silver nanoparticles, zinc oxide nanoparticles, and silver-zinc oxide nanocomposites using Pistacia Atlantica Resin. *Mater. Today Commun.* **2021**, 27, 102457.
16. Khani, R.; Roostaei, B.; Bagherzade, G.; Moudi, M. Green synthesis of copper nanoparticles by fruit extract of *Ziziphus spina-christi* (L.) Willd.: Application for adsorption of triphenylmethane dye and antibacterial assay. *J. Mol. Liq.* **2018**, 255, 541-549.
17. Tanvir, F.; Yaqub, A.; Tanvir, S.; Anderson, W.A. Poly-L-arginine coated silver nanoprisms and their anti-bacterial properties. *Nanomaterials* **2017**, 7, 296.
18. Sardar, R.; Shumaker-Parry, J.S. Spectroscopic and microscopic investigation of gold nanoparticle formation: ligand and temperature effects on rate and particle size. *J. Am. Chem. Soc.* **2011**, 133, 8179-8190.
19. Yang, H.; Jiang, F.; Zhang, L.; Wang, L.; Luo, Y.; Li, N.; Guo, Y.; Wang, Q.; Zou, J. Multifunctional L-arginine-based magnetic nanoparticles for multiple-synergistic tumor therapy. *Biomater. Sci.* **2021**, 9, 2230-2243.
20. Ma, Y.; Pitt, J.M.; Li, Q.; Yang, H. The renaissance of anti-neoplastic immunity from tumor cell demise. *Immunol. Rev.* **2017**, 280, 194-206.
21. Salimi, E.; Nigje, A.K. Investigating the antibacterial activity of carboxymethyl cellulose films treated with novel Ag@ GO decorated SiO_2 nanohybrids. *Carbohydr. Polym.* **2022**, 298, 120077.
22. Bharathi, D.S.; Boopathyraja, A.; Nachimuthu, S.; Kannan, K. Green synthesis, characterization and antibacterial activity of SiO_2–ZnO nanocomposite by *Dictyota bartayresiana* extract and its cytotoxic effect on HT29 Cell Line. *J. Cluster Sci.* **2022**, 33, 2499-2515.
23. Zamani, L.; Faghih, Z.; Zomorodian, K.; Mirjalili, B.B.F.; Jalilian, A.; Khabnadideh, S. Nano-$SnCl_4.SiO_2$, an efficient catalyst for synthesis of benzimidazole drivatives as antifungal and cytotoxic agents. *Res. Pharm. Sci.* **2019**, 14, 496.
24. Roberson, M.; Rangari, V.; Jeelani, S.; Samuel, T.; Yates, C. Synthesis and characterization silver, zinc oxide and hybrid silver/zinc oxide nanoparticles for antimicrobial applications. *Nano Life* **2014**, 4, 1440003.
25. Elumalai, K.; Velmurugan, S. Green synthesis, characterization and antimicrobial activities of zinc oxide nanoparticles from the leaf extract of *Azadirachta indica* (L.). *Appl. Surf. Sci.* **2015**, 345, 329-336.
26. Shahabadi, N.; Akbari, A.; Karampour, F.; Falsafi, M.; Zendehcheshm, S. In vitro cytotoxicity, antibacterial activity and HSA and ct-DNA interaction studies of chlorogenic acid loaded on γ-Fe_2O_3@ SiO_2 as new nanoparticles. *J. Biomol. Struct. Dyn.* **2022**, doi: 10.1080/07391102.2022.2030799.
27. Shaikh, S.; Nazam, N.; Rizvi, S.M.D.; Ahmad, K.; Baig, M.H.; Lee, E.J.; Choi, I. Mechanistic insights into the antimicrobial actions of metallic nanoparticles and their implications for multidrug resistance. *Int. J. Mol. Sci.* **2019**, 20, 2468.
28. Amirnejat, S.; Nosrati, A.; Javanshir, S.; Naimi-Jamal, M.R. Superparamagnetic alginate-based nanocomposite modified by L-arginine: An eco-friendly bifunctional catalysts and an efficient antibacterial agent. *Int. J. Biol. Macromol.* **2020**, 152, 834-845.
29. Nassar, M.Y.; El-Salhy, H.I.; El-Shiwiny, W.H.; Abdelaziz, G.; El-Shiekh, R. Composite nanoarchitectonics of magnetic silicon dioxide-modified chitosan for doxorubicin delivery and in vitro cytotoxicity assay. *J. Inorg. Organomet. Polym. Mater.* **2022**, 396, 1-17.